Vertical Distribution of PH_3 in Saturn from Observations of the 1-0 and 3-2 Rotational Lines

Glenn S. Orton
M. S. 169-237
Jet Propulsion Laboratory
4800 Oak Grove Drive Pasadena, CA 91109

E. Serabyn
M. S. 171-113
Jet Propulsion Laboratory
4800 Oak Grove Drive Pasadena, CA 91109

Y. T. Lee
M. S. 150-21
Division of Geological and Planetary Sciences
Cailfornia Institute of Technology
Pasadena, CA 91125

May 14, 1999

Short title: *Phosphine in Saturn*
Submitted to: *Icarus*
Figures: 12
Tables: 0
Send correspondence to:
Glenn S. Orton, JPL 169-237, 4800 Oak Grove Dr., Pasadena, CA 91109.
go@orton.jpl.nasa.gov
Key words: **atmospheres**, composition; **photochemistry**; **Saturn**, atmosphere; spectroscopy

Abstract

Far-infrared Fourier-transform spectrometer measurements of the 1-0 and 3-2 PH_3 transitions in Saturn's disk near 267 and 800 GHz (8.9 and 26.7 cm^{-1}), respectively, were analyzed simultaneously to derive a global mean profile for the PH_3 vertical mixing ratio between 100 and 800 mbar total pressure. The far-infrared spectrum is relatively free from spectral interlopers, suffers minimal absorption or scattering by atmospheric particulates, and contains fairly weak PH_3 lines that are sensitive to a range of atmospheric depths. The combined spectra are inconsistent with a constant tropospheric mixing ratio, even with a stratospheric cut-off. They are consistent with a volume mixing ratio of PH_3 that drops from 1 x 10^{-5} at 800 mbar pressure to a value of 4 x 10^{-7} at 100 mbar pressure, connected by the expression 3.21 x 10^{-10} $p^{1.55}$, for p in mbar. This expression is consistent with the data, even when extended to pressures higher than 800 mbar and pressures lower than 100 mbar. The mixing ratio could drop even more quickly at atmospheric pressures below 100 mbar and still be consistent with the data, and the mixing ratio could also remain constant with depth at a value near 7 x 10^{-6} for pressures above 630 mbar. If the mixing ratio does not decrease in value with depth, then the highest values in the best fit model imply a [P]/[H] ratio that is well above the solar ratio. The falloff feature of the PH_3 mixing ratio in the upper troposphere is sensitive to the eddy diffusion coefficient above the 1-bar level. Photochemical models of PH_3 provide an estimate of eddy diffusion coefficient in this region of the atmosphere to be somewhere between 10^5 to 10^6 cm^2 sec^{-1}.

Introduction

The presence of phosphine in Jupiter and Saturn was not expected in detectable amounts on the basis of equilibrium thermochemical considerations. PH_3 is not chemically stable at temperatures below ~500 K (Prinn and Lewis 1975). At the low (<150 K) temperatures of the sensible atmospheres of these planets, the PH_3 abundance is expected to drop as solid phosphorus precipitates are formed (Fegley and Lodders 1994, Borunov *et al.* 1995). The presence of PH_3 in detectable quantities is most readily explained by assuming that it is mixed upward from the deeper, warmer atmosphere faster than it decomposes chemically. Because of this, PH_3 can act as a tracer for chemical and dynamical properties of the atmosphere.

Phosphine was first suspected as a major influence on Saturn's spectrum by Gillett and Forrest (1974) and was confirmed by high-resolution spectroscopic detection by Bregman *et al.* (1975). Fink and Larson (1977) further confirmed the presence of PH_3 in Saturn through its influence on the 5-μm spectrum. The first quantitative mixing ratio was derived by Tokunaga *et al.* (1980,1981). They derived a value between 0.8 to 1.6 x 10^{-6} and required that the vertical distribution undergo a sharp cutoff at total pressures below 100 mbar in order to avoid emission cores in the strongly absorbing centers of lines which otherwise sampled the warm "inverted" stratosphere. Using Voyager IRIS spectra from the northern hemisphere, Courtin *et al.* (1984) derived a constant value of 1.45±0.8 x 10^{-6} for the PH_3 mixing ratio (assuming a mixing ratio of 96% for H_2 after Conrath *et al.* 1984) with a cutoff at pressures lower than 3 mbar. They also noted that the analysis of International Ultraviolet Explorer observations conducted by Winkelstein *et al.* (1983) required a cutoff of the PH_3 mixing ratio at pressures lower than 25 mbar. Many of these results are summarized in Table IV and Fig. 6 of Prinn *et al.* (1984).

Since the time of that review, Noll and Larson (1990) observed and analyzed Saturn's 5-μm spectrum, including a determination of the PH_3 mixing ratio. They fixed its value at 1 x 10^{-6}, in agreement with previous work, for levels of the atmosphere where the total pressures was less than 400 mbar. This value was consistent with the portion of the spectrum dominated by reflected sunlight. They derived a mixing ratio of 7 x 10^{-6} for pressures greater than 400 mbar, using a

portion of the spectrum dominated by thermal emission.

All these early results were due to analyses of vibrational-rotational lines. The "pure" rotational far-infrared 1-0 transition at 266.9 GHz was first observed and analyzed by Weisstein and Serabyn (1994). They found a constant tropospheric mixing ratio of 3 ± 1 x 10^{-6} to be consistent with the depth and shape of the 1-0 line. In order to avoid the appearance of an "emission core" in this line arising from Saturn's relatively warm stratosphere, they also required a high-altitude cutoff somewhere between 13 and 140 mbar total pressure, above which no PH_3 was present. The utility of this line is that is it sensitive to regions of the atmosphere that are significantly deeper than the levels to which the middle-infrared vibration-rotation lines are sensitive. Weisstein and Serabyn (1996) also reported the detection of the 3-2 PH_3 transition at 800.5 GHz, although the anlysis of this line was deferred to a subsequent publication. That is, of course, the motivation for the current report.

Even more recently, observations of Saturn were obtained by the Infrared Space Observatory Short Wavelength Spectrometer (SWS) and Long Wavelength Spectrometer (LWS). The most prominent features in the LWS spectra of Saturn between 43 and 197 μm are pure rotational lines of PH_3, all of which have greater strengths than the two lines reported by Weisstein and Serabyn (1994, 1996). The spectra were fit using a constant tropospheric mixing ratio of 7 x 10^{-6} for pressures greater than 300 mbar, with negligible amounts at lower presures (Davis *et al.* 1996). Unfortunately, the value of the constant mixing ratio that Davis *et al.* derived is incorrect, as it is based on spectroscopic line parameters taken from the GEISA data base (Husson *et al.* 1994) that has incorrect line intensities for PH_3 rotational lines (Bézard, pers. comm.) The re-analysis of the ISO/LWS data is ongoing. The ISO/SWS data are consistent with a mixing ratio of 2.5 x 10^{-6} at 300 mbar, assuming (1) a value of 4.5 x 10^{-6} at the 600-mbar level and deeper in the atmosphere, and (2) a dropoff from the 300-mbar level to a value of 1 x 10^{-9} at 150 mbar (de Graauw *et al.* 1997). The mixing ratios between these levels are linearly interpolated in logarithmic form vs log of pressure.

Observations

The spectroscopic observations of the 1-0 and the 3-2 lines reported by Weisstein *et al.* (1994, 1996) form the basis of this paper. Both lines are illustrated in Fig. 1. For this analysis, the spectra were processed further. For the 1-0 line, the ripple seen in Fig. 4 of Weisstein and Serabyn (1994) was removed by fitting a single-frequency sine wave component to the spectrum. This dramatically cleaned up the spectrum in the vicinity of the 1-0 line (Fig. 1) but made the more distant baseline noisier where the sine wave fit is no longer applicable. The 3-2 line lies near the edge of an atmospheric window and is very broad. Thus, the high-frequency line wing extends across most of the spectral region observed, and most of the distant low-frequency line wing is completely obscured by the terrestrial atmosphere. In addition, the accessible part of the low-frequency wing is likely to be somewhat affected by rapidly dropping atmospheric and instrumental transmission. The baseline is thus difficult to determine. Finally, slight (0.5-GHz) offsets in line frequencies seem to be present. These could arise from imperfect subtraction of the sine wave component in the 1-0 line or an uncorrected baseline curvature below 800 GHz in the 3-2 line, or, less likely, a possible contribution by HCN. However, the absence of other HCN features rules this possibility out.

Fig. 1

The radiance of the 1-0 data were determined by cross-calibration with Venus (Weisstein *et al.* (1994). The 270-GHz continuum brightness temperature of 144 Kelvins derived by Weisstein and Serabyn (1984) agrees with earlier broadband measurements (see their Table II) by Courtin *et al.* (1977), Ulich *et al.* (1984) and Werner *et al.* (1978). In this spectral region, the very low temperature of Saturn's rings (*cf.* Fig. 3 of Roellig *et al.* 1988), implies that they do not contribute significantly to the total observed radiance. For the 3-2 data near 800 GHz, on the other hand, determining the true continuum radiance, for which a calibration body was not available (Weisstein *et al* 1996), requires us to fit only the shapes of the two lines simultaneously, shifting the continuum as required by the model. Nevertheless, there is considerable information from prior studies that provides useful constraints on the absolute continuum in this spectral region. Our models indicate that the continuum brightness in the 800-GHz region is fixed by our choice of temperature profile (see below). Our choice appears to be consistent with the results of broadband continuum mea-

surements by Loewenstein *et al.* (1977), Cunningham *et al.* (1981) and Hildebrand *et al.* (1985) with continuum brightness temperatures that all fall in the range of 97 - 103 Kelvins. Although measurements by Roellig *et al.* (1988) indicate a brightness temperature for the rings of some 40 Kelvins, the mere 6° opening of the rings mitigates against them providing a significant contribution to the spectrum, particularly as any continuum is subsumed in the planetary continuum after normalization to the model brightness temperature.

Model Basis

A radiative transfer code was employed to derive synthetic spectra to match the observations. The code used 20 vertical layers per decade of pressure, with a linear-in-τ approximation for the variation of the source function within each layer. A 5-stream Gaussian quadrature grid in the emission angle cosine was used to integrate the disk-averaged flux. Tests confirmed that the cloud opacities derived for Saturn, even for large ($\lambda > 1$ μm) particles (*e.g.* Orton 1983) did not exert a significant influence on the upwelling radiance. Atmospheric opacities for this model are given in detail below.

Part of the continuum opacity of Saturn's infrared spectrum arises from the collision-induced dipole of H_2, as influenced by H_2 and He collisions. The collision-induced opacity was modeled following Birnbaum *et al.* (1996). The mixing ratios of H_2 and He were assumed to be 96% and 4%, respectively (Conrath *et al.* 1984).

A detailed, line-by-line code was used to integrate over discrete molecular transitions. Transition frequencies, line strengths and ground state energies for these molecules were taken from the spectral line catalog of Pickett *et al.* (1992). The line widths for NH_3 pressure-broadened by H_2 and their temperature dependences were taken from Brown and Peterson (1994) and reduced by 10% as an approximation to the influence of He broadening. The shape of NH_3 inversion lines broadened by H_2 were modeled using the "modified Ben-Reuven" form derived by Berge and Gulkis (1976), except that their single value for H_2 broadened line widths were replaced by the Brown and Peterson values. The shape of the rotational NH_3 lines broadened by H_2 was modeled using the line coupling derived by Birnbaum *et al.* (1998). The pressure-broadened line widths for PH_3 broadened by H_2 and He

were taken from a general formula given by Levy *et al.* (1993), their temperature dependence was taken from Levy *et al.* (1994), and VanVleck-Weiskoff lineshapes were assumed.

The disk-averaged temperature profile was taken from the Infrared Space Observatory Short-Wavelength Spectrometer investigation of Saturn's disk-averaged structure and composition (*e.g.* Bézard *et al.* 1998), kindly supplied by Bruno Bézard (Fig. 2). This profile was chosen over earlier ones as it averaged over the entire disk, similar to our observations, rather than being applicable to a specific region or regions of the planet, such as the Voyager IRIS experiments (*e. g.* Conrath and Pirraglia 1983) or the Voyager radio occultation experiment (Lindal *et al.* 1987). Fig. 2

The mixing ratio of NH_3 below total pressures of about 1 bar (temperatures less than 135 K) is taken to be the saturated mixing ratio above the ammonia condensation level, consistent with various studies in the thermal infrared (*e.g.* Courtin *et al.* 1984). However at higher pressures and temperatures, and deeper than the condensation level, the abundance is a significant opacity source for the ~280 GHz spectral region. Because of the difficulty of sounding this region through cloud cover in the infrared, NH_3 abundances have been determined from the submillimeter through radio spectrum. The NH_3 mixing ratio profile has been given by (i) dePater and Massie (1985) as 5×10^{-4} for $p > 3$ bar and 3×10^{-5} for $p < 1.25$ bar, (ii) Briggs and Sackett (1989) as $4 - 6 \times 10^{-4}$ for p~25 bar and decreasing to $0.7 - 1.1 \times 10^{-4}$ for p~2 bars, and (iii) Grossman *et al.* (1989) as 1.2×10^{-4} just below the condensation level. With so little detailed agreement on the NH_3 mixing ratio just below the clouds, we somewhat arbitrarily selected a nominal mixing ratio of 1×10^{-4} below the condensation level.

The sensitivity of the spectrum to the value of the NH_3 mixing ratio is shown by the dotted curves that envelope the nominal spectrum. These upper and lower limits correspond to values between 3×10^{-5} (upper curve) and 4×10^{-4} (lower curve). Note that the continuum far from the PH_3 1-0 line does not vary significantly even if the PH_3 mixing ratio is varied a factor of ~2 (the difference between the solid and dashed curves in Fig. 1). Furthermore, the continuum far from the PH_3 3-2 line is influenced neither by variations of the PH_3 nor of the NH_3 mixing ratios in the deep atmosphere. Therefore, the only consequence of changing the NH_3 mixing ratio in the

deep atmosphere is to change the continuum level in the 280-GHz region away from its observed levels. We retain the nominal deep NH_3 mixing ratio of 1 x 10^{-4}, understanding that the value is uncertain by factors of ~3 - 4, but that the nominal value is consistent with the independently measured continuum radiances in the 280-GHz region discussed earlier.

PH_3 Models

Originally the 1-0 PH_3 line was fit by a constant tropospheric mixing ratio of 3 x 10^{-6} with a stratospheric cutoff (Weisstein and Serabyn 1994). However, we found the spectrum of the 3-2 line to be inconsistent with this mixing ratio. The primary observations indicate very different widths for the two lines: 10 GHz at 267 GHz *vs* 25-30 GHz at 805 GHz. To illustrate the problem, we tested two simple vertical distributions of PH_3.

If we change the value for the tropospheric mixing ratio of PH_3 to 1.8 x 10^{-6}, Fig. 1 shows that it works reasonably well in the distant wings and at the centers of the 1-0 line and 3-2 lines. However, this model is clearly warmer than the data in the "near wings" of the 1-2 lines and somewhat colder than the 3-2 lines near their half-power frequencies. On the other hand, a model with a tropospheric PH_3 mixing ratio of 4 x 10^{-6} does well in the distant and "near" wings of the 1-0 line, but it is colder than the center of that line, and it is colder than the wings of the 3-2 line. Thus, a single mixing ratio is inappropriate.

Both models cut off the PH_3 distribution just above the 100-mbar level. This allows no emission to arise from the thermally "inverted" hot stratosphere. Figure 1 shows that, as a result, no emission core appears at the center of the strong 3-2 line. In fact, making this assumption, the brightness temperature of Saturn at this line center is controlled only by the assumed value of the temperature minimum. On the other hand, the brightness temperatures in the continuum is controlled only by H_2 opacity and so is also fixed. Thus, the radiance of the 800-GHz spectrum is fixed by the choice of the temperature structure in two ways, matching the brightness temperature of the line center, and of the distant continuum. It turns out that a single scaling matches both quantities fairly well. The reasonable agreement between the models and the data both at the center of the line, as well as the distant wings of the line, thus attests to the general appropriateness of the chosen

temperature structure, as well as to the accuracy of the fundamental measured quantity, the line to continuum ratio.

Since the 1-0 line arises from deeper levels than the 3-2 line, a better model would decrease the PH_3 mixing ratio with altitude. In fact, we can adopt a model in which the mixing ratio varies continuously as a function of pressure throughout the entire vertical range to which our measurements are sensitive, using a linear relationship between the logarithm of the mixing ratio and the logarithm of the pressure. This model is shown in Fig. 3, and the mixing ratio in this relationship can be expressed as a power law in pressure: $3.2 \times 10^{-10}\ p^{1.55}$, for p in mbar. This model is the result of a least-squares fit to the data that define the lines. The fit of this model to the data is shown in Fig. 4. Figs. 3 and 4 illustrate the minimal sensitivity of the model to the level of the cutoff of the abundance near the tropopause. Clearly the cutoff must be at a pressure lower than 250 mbar, but it could easily be at pressures as high as 100 mbar. Conversely, extrapolating the rapid tropospheric falloff into the stratosphere with cutoffs at pressures as low as 1 - 10 mbar (not visible in Fig. 3 but present in Fig. 4) does not produce model spectra in conflict with our data. Because of the assumed rapid vertical falloff, the mixing ratio in the warm stratosphere is insufficient to produce an "inversion core" at the center of the 3-2 line. We will adopt this profile as our nominal model, using the relationship given above to define the PH_3 mixing ratio for all pressures down to 10 mbar.

Fig. 3

Fig. 4

This simple model does not provide perfect fits to both spectral regions simultaneously. In fact, there is a direct tradeoff between the quality of the fit to the spectrum at the 1-0 line and in the wings of the 3-2 line. A larger mixing ratio near the 200-mbar level (temperatures near 110 K) would produce a better fit to the PH_3 1-0 line, but it would make the fit to the 3-2 line worse in the 812 - 828 GHz region. This overlap between the vertical sensitivities of these two regions is illustrated in Fig. 5 which shows the weighting functions associated with the outgoing radiances in the center and mid-wings of the two lines. The radiance at 267 GHz and at 812 and 818 GHz all arise from the ~200-mbar pressure level. Nevertheless, limitations in these initial observations, such as the subtracted sine wave ripple in the 1-0 line and the low transmission below ~790 GHz,

Fig. 5

make these models acceptable at this point. Our inability to provide a perfect fit to both spectral regions simultaneously, together with the level of random noise, result in an uncertainty of some 25% in the value of the mixing ratio, illustrated in Fig. 3 by the horizontal bars.

We note that if the NH_3 mixing ratio were changed by as much as factors of 4, in line with its uncertainty (as discussed above), the 280-GHz portion of the spectrum would need to be scaled upward, and a new brightness scale would have to be established for the 3-2 line. Such a change would require a 20% adjustment in the PH_3 mixing ratio in the 400-800 mbar pressure range, and that must be considered a source of systematic uncertainty. Arguing against this, of course, is the fact that the nominal mixing ratio for NH_3 fits the independently measured continuum radiance spectrum quite well.

Fig. 5 also illustrates the range of depths to which we are sensitive, approximately 100 to 600 mbar. The 1-0 line, in particular, is a very good probe for the PH_3 abundance at depth. Note that even higher J rotational lines of PH_3 will arise from higher in the atmosphere than even the 3-2 line and will, therefore, be sensitive to the mixing ratio of PH_3 near the 100-mbar level. It is thus the lowest 1-0 line that provides us with information from deepest in the atmosphere.

We undertook to improve the model by inverting the spectral data and solving for the abundance of PH_3 as a function of depth between 100 and 630 mbar, using the generalized remote sensing inversion approach of Chahine (1970) and the nominal model as an initial guess. The results, in fact, were not significantly different from those of the nominal model, and only a 25% improvement in the residuals to the data were achieved.

We also checked the results after perturbing the temperature structure. If the temperature profile is lowered by 2 K, the spectrum can then be fit to the same level by lowering the PH_3 mixing ratio by 25% uniformly (Fig. 6). The results are, in fact, somewhat better than the nominal model at the center of the 3-2 line, but otherwise the results are nearly the same as the nominal model spectrum. Fig. 6

Finally, we point out that, while two transition of HCN are within our spectral range (265.8 and 797.4 GHz), tests show that they would be detectable above our noise level only if the upper

tropospheric mixing ratios were greater than or equal to 3 x 10^{-9}. That is significantly higher than the upper limit of the HCN mixing ratio of 4 x 10^{-10} derived by Weisstein and Serabyn (1996).

Discussion

Our nominal model for the global average of the vertical distribution of PH_3 in Saturn is shown in Fig. 7, the solid line highlighting the approximate vertical range to which we are sensitive. Fig. 7
Above the ~0.1-bar level, we lose sensitivity because of the isothermal nature of the temperature structure. The steep linear dropoff of our model does not create an emission core in the 3-2 PH_3 line above our noise level. Furthermore, it is consistent with the low PH_3 abundance required by Winkelstein *et al.* (1983) above the 25-mbar level in order to match Saturn's 180 - 220 nm spectrum recorded by the International Ultraviolet Explorer. The profile is a bit higher than the PH_3 mixing ratio upper limits derived from Hubble Space Telescope Faint-Object Spectrograph data for latitudes at and poleward of 36°N (Edgington *et al.* 1998), and it is possible that our whole-disk observations are dominated by the signatures of the PH_3 vertical profile for low-latitude regions. Our data are also insensitive to the mixing ratio deeper than the 800-mbar pressure level, as shown by the alternative line at a constant mixing ratio of ~7 x 10^{-6} which results in no change to our spectrum.

The PH_3 vertical distribution derived by Courtin *et al.* (1984) (Fig. 7) is not consistent with our data. Similar to all models with a constant mixing ratio in the troposphere (*e.g.* Tokunaga *et al.* 1980, 1981), it cannot fit both our observed lines simultaneously. Furthremore, its constant PH_3 mixing ratio of 1.45 x 10^{-6} up to the 3-mbar level (where the stratospheric temperature is ~130 K in our model) produces an unmistakable emission core that is well above our noise level (Fig. 8). Fig. 8

The PH_3 distribution used to model the ISO/SWS middle-infrared spectrum of Saturn (de-Graauw *et al.* 1997) is also shown in Fig. 7. It is not quite a distributed uniformly in the troposphere, but the mixing ratio deeper than the ~400-mbar pressure level is too low to fit either of the 1-0 or 3-2 lines (Fig. 8).

Noll and Larson's (1990) vertical distribution was the only nonuniform tropospheric vertical

distribution of PH_3 based on measurement constraints in the literature prior to the ISO mission. While employing a crude stepfunction at the 400-mbar level, it nevertheless appears close to the values in our smoother distribution (Fig. 9), and its spectrum does reasonably well at matching our 3-2 observations. However, changing the location of the step to the 500-mbar level, and increasing the value of the deeper mixing ratio from 7 x 10^{-6} to 2.2 x 10^{-5}, achieves a fit to both lines that is generally as good as our nominal model (Fig. 10). Fig. 9 Fig. 10

One main conclusion of our work is that the deep atmospheric mixing ratio of PH_3 must be at least 7 x 10^{-6}. The value could also be higher. Our data do not constrain the mixing ratio deeper than the 800-mbar level, and a further increase with depth would be perfectly consistent with our data. This deep PH_3 mixing ratio implies a [P]/[H] abundance ratio that is at least 10 times the one expected from the solar ratio, consistent with Noll and Larson's (1990) results.

It also appears both from our data and from the 5-μm spectrum of Saturn, that the PH_3 vertical distribution drops sharply with altitude in the upper troposphere of Saturn. The question that remains is the origin of this effect: is the dropoff the result of increased chemical scavenging with height, disequilibrium tropospheric chemistry, or photodissociation, given that Saturn is too warm for PH_3 condensation.

Qualitatively, the dropoff has the morphology of the vertical distribution of NH_3 in Jupiter for pressures less than 8 bars at the Galileo probe entry site as determined by the attenuation of the probe relay antenna (Folkner *et al.* 1998). However, unlike PH_3, NH_3 is a condensate in both Jupiter and Saturn, and it is also subject to chemical scavenging by H_2S. In addition, the Galileo probe entered the atmosphere in an unusually clear and possibly dry, downwelling region (Orton *et al.* 1998) that may not be at all characteristic of the average conditions on the planet. In fact, there are few established theoretical reasons to support any specific chemical mechanisms for removing PH_3 from the atmosphere are effective at the atmospheric levels where we see the falloff.

The tropospheric chemistry of PH_3 has been modeled by Prinn *et al.* (1984), Prinn and Fegley (1985) and Fegley and Lodders (1994). All of the models show that PH_3 is subject to a reaction with H_2O to form P_4O_6 and molecular hydrogen. For conditions of thermochemical equilibrium,

at the temperatures to which our spectra are sensitive, the mixing ratio of PH_3 should be orders of magnitude lower than detected, with the reaction favoring P_4O_6 below temperatures of about 950 K. For temperatures below 404 K, condensation of $CH_4H_2PO_4$(s) decreases the abundance of gaseous P_4O_6 (*cf.* Fig. 3 of Fegley and Prinn, 1985). The timescale for establishing equilibrium chemistry, therefore, must be much longer than the timescale for vertical mixing. The temperature at the level where chemical equilibrium is taking place at a rate equal to the vertical mixing rate is known as the "quench temperature", estimated by Prinn *et al.* as close to 1200 K. Above this level in Saturn, the vertical mixing is sufficiently rapid that the mixing ratio of PH_3 is essentially constant. Fig. 33 of Fegley and Lodders (1994), plots the PH_3 mixing ratio expected to be observable in the upper troposphere *vs* the vertical eddy diffusion coefficient. It is possible, of course, to envision that the time scale for vertical mixing increases dramatically toward the tropopause, together with the static stability of the atmosphere against buoyancy. However, these levels of the atmosphere are far above the condensation level for H_2O (several bars of pressure), and the extremely low mixing ratio of H_2O makes the efficacy of PH_3 oxidation reactions an unlikely cause for its depletion.

The alternative is, of course, photochemical destruction of PH_3. To test the photochemical removal of PH_3 in the upper troposphere, and the impact of varying vertical motion in this region, we use the Caltech/ JPL 1-D photochemical model to solve photochemical reactions and dynamical transport of PH_3 and other relevant species in each pressure level. This model incorporates PH_3 and NH_3 photochemical reactions, molecular and bulk atmospheric vertical motions, condensation of NH_3 below the tropopause, and the attenuation of solar radiation by absorption and scattering. There are three photochemical reactions that can remove PH_3 by decomposition in this model:

$$PH_3 + h\nu \rightarrow PH_2 + H \quad \text{(R1)}$$

$$PH_3 + H \rightarrow PH_2 + H_2 \quad \text{(R2)}$$

$$PH_3 + NH_2 \rightarrow PH_2 + NH_3 \quad \text{(R3)}$$

The major band of ultraviolet radiation for reaction R1 is < 200 nm, which is mostly shielded by CH_4 and NH_3 in the upper atmosphere. Therefore, the photolysis of PH_3 in the troposphere of

Saturn is not expected to be the dominant mechanism. However, chemical decomposition of PH_3 by either H or NH_2 radicals may be more important.

Vertical motion is sensitive to the abundance of PH_3 in the upper troposphere, as pointed out by Kaye and Strobel (1984). The characteristic vertical motion is conventionally parameterized as eddy diffusion coefficient, in units of $cm^2\ sec^{-1}$. Eddy diffusion coefficient corresponds to the macroscopic bulk atmospheric vertical motion. For the purpose of testing the sensitivity of varying eddy diffusion coefficients, we choose five values, 10^3, 10^4, 10^5, 10^6, and $10^7\ cm^2\ sec^{-1}$, as different cases in this model. In each case, we fix the PH_3 mixing ratio of 1 x 10^{-5} at the 1-bar pressure level as the boundary condition. We also assume a uniform eddy diffusion coefficient vertical profile, from the 1-bar to the 100-mbar levels, for simplicity. The model results of the five eddy diffusion coefficient cases are shown in Fig. 11. It is obvious that in the higher vertical motion case (K = $10^7\ cm^2\ sec^{-1}$), PH_3 is distributed all the way to the tropopause with uniform mixing ratio. On the other hand, the slow vertical motion case (K = $10^3\ cm^2\ sec^{-1}$) does not supply the quantities of PH_3 that we measured. The PH_3 mixing ratio profile that we derive in this work is consistent with an eddy diffusion coefficient in the upper troposphere that is between about 10^5 and $10^6\ cm^2\ sec^{-1}$. Fig. 11

If the photochemical destruction of PH_3 is responsible for its depletion in the upper troposphere, what reaction is primarily responsible? The R1, R2 and R3 reaction rate profiles are shown in Fig. 12. These profiles are derived from the steady-state solution for the photochemical model where K = $10^5\ cm^2\ sec^{-1}$. Photolysis by solar UV radiation only contributes the loss mechanism around the tropopause. PH_3 destruction by NH_2 radical attacking is important in the region above the 300-mbar level, according to the large amount of NH_2 produced by NH_3 photolysis. Deeper in the troposphere, destruction by H atoms dominates. Fig. 12

Edgington *et al.* (1998) find that the maximum PH_3 mixing ratios allowed by their spectra in Saturn's lower stratosphere depend on latitude. Extending such studies down into the troposphere could be done using a high-resolution spectrometer that covers the PH_3 3-2 and 1-0 submillimeter lines. The spectra from such an instrument would constrain models for the vertical wind regime

of the atmosphere as a function of latitude. Until such an instrument is deployed, however, we can use techniques that detect both moderate and weak PH_3 lines at shorter wavelengths, even without resolving the individual line shapes, coupled with appropriate cloud models from accurate continuum measurements. Although they will not be sensitive down as deep as the 800-mbar level, such observations will be made by both the Cassini Visible and Infrared Mapping Spectrometer (VIMS) and the Composite Infrared Spectrometer (CIRS) experiments, although they will not be sensitive down as deep as the 800-mbar level. Only a direct probe of Saturn's atmosphere is likely to be successful in determining the PH_3 mixing ratio deeper than the 800-mbar level.

Acknowledgements

We are grateful for helpful discussions with Mark Allen, Sushil Atreya, and Darryl Strobel on the current status of ultraviolet constraints and the current state of photochemical models for PH_3 in Saturn, and to Ed Cohen for describing details of the Pickett and Poynter submillimeter line catalog for PH_3. We thank Bruno Bézard for a digital version of his disk-averaged temperature profile for Saturn that was derived from ISO/SWS data. This work was supported by research grants to the Jet Propulsion Laboratory and the California Institute of Technology from the Planetary Astronomy and Planetary Atmospheres disciplines of the Office of Space Science and Applications of the National Aeronautics and Space Administration.

References

Berge, G. L. and S. Gulkis. 1976. Earth-based radio observations of Jupiter: Millimeter to meter wavelengths. In Jupiter, T. Gehrels, Ed. Univ. of Arizona Press, Tucson. pp. 621-692.

Bézard, B., H. Feuchtgruber, J. I. Moses, and T. Encrenaz. 1998. Detection of methyl radicals (CH_3) on Saturn. *Astron Astrophys.* **334**, L41 - L44.

Birnbaum, G., A. Borysow, and G. S. Orton. 1996. Collision-induced absorption of H_2-H_2 and H_2-He in the rotational and fundamental band for planetary applications. *Icarus* **123**, 4 - 22.

Birnbaum, G., A. Buechele, T. Jian, G. S. Orton, Z. Hadzibabic, and G. R. John. 1999. Absorption in the troughs of the far infrared spectra of NH_3 and mixtures of NH_3 and H_2. *J. Quant. Spectrosc. Radiat. Transf.* In press.

Borunov, S., V. Dorofeeva, I. Chodakovsky, P. Drossart, E. Lellouch, and T. Encrenaz. 1995. Phosphorus chemistry in the atmosphere of Jupiter: A reassessment. *Icarus* **113**, 460 - 464.

Bregman, J. D., D. F. Fester, and D. M. Rank 1985. Observation of the ν_2 band of PH_3 in the atmosphere of Saturn. *Astrophys. J. Lett.* **202**, L55 - L56.

Briggs, F. H. and P. D. Sackett. 1989. Radio observations of Saturn as a probe of its atmosphere and cloud structure. *Icarus* **80**, 77-103.

Brown, L. R. and D. B. Peterson. 1994. An empirical expression for linewidths of ammonia from far-infrared measurements. *J. Molec. Spectrosc* **168**, 593 - 606.

Chahine, M. T. 1970. Inverse problems in radiative transfer: Determination of atmospheric parameters. *J. Atmos. Sci* **27**, 960 - 967.

Conrath, B. J. and J. A. Pirraglia. 1983. Thermal structure of Saturn from Voyager infrared measurements: Implications for atmospheric dynamics. *Icarus* **53**, 286-292.

Conrath, B. J. D. Gautier, R. A. Hanel, and J. S. Hornstein. 1984. The helium abundance of Saturn from Voyager measurements. *Astrophys. J.* **282**, 807 - 815.

Courtin, R. N. Coron, T. Encrenaz, R. Gispert, P. Bruston, J. Leblanc, G. Dambier, and A. Vidal-Madjar. 1977. Observations of giant planets at 1.4 mm and consequences on the effective temperatures *Astron. Astrophys.* **60**, 115 - 123.

Courtin, R., D. Gautier, A. Marten and B. Bézard. 1984. The composition of Saturn's atmosphere at northern temperate latitudes from Voyager IRIS spectra: NH_3, PH_3, C_2H_2, C_2H_6, CH_3D, CH_4. *Astrophys. J.* **287**, 899 - 916.

Cunningham, C. T, P, A. R. Ade, E. I. Robson, I. G. Nolt and J. V. Radostitz. 1981. The submillimeter spectra of the planets: Narrow-band photometry. *Icarus* **48**, 127 - 139.

Davis, G. R., M. J. Griffin, D. A. Naylor, P. G. Oldham, B. M. Swinyard, P. A. R. Ade, S. B. Calcutt, T. Encrenaz, T. de Graauw, D. Gautier, P. G. J. Irwin, E. Lellouch, G. S. Orton, C. Armand, M. Burgdorf, A. DiGiorgio, D. Ewart, C. Gry, K. J. King, T. Lim, S. Molinari, M. Price, S. Sidher, A. Smith, D. Texier, N. Trams, S. J. Unger. 1996. ISO LWS measurement of the far-infrared spectrum of Saturn. *Astron. Astrophys.* **315**, L393-396.

dePater, I.and S. T. Massie. 1985. Models of the millimeter-centimeter spectra of the giant planets. *Icarus* **62**, 143-171.

Edgington, S. G., S. K. Atreya, L. M. Trafton, J. J. Caldwell. R. F. Beebe, A. A. Simon, R. A. West, and C. Barnet. 1998. Phosphine mixing ratios and eddy mixing coefficients in the troposphere of Saturn. *Bull. Amer. Astron. Soc.* **29**, 992.

Fegley, B. and R. G. Prinn. 1985. Equilibrium and nonequilibrium chemistry of Saturn's atmosphere - Implications for the observability of PH_3, N_2, CO and GeH_4. *Astrophys. J.* **299**, 1067 - 1078.

Fegley, B., Jr. and K. Lodders. 1994. Chemical models of the deep atmospheres of Jupiter and Saturn. *Icarus* **110**, 117 - 154.

Fink, U. and H. P. Larson. 1977. The 5 μ spectrum of Saturn. *Bull. Amer. Astron. Soc.* **9**, 535.

Folkner, W. M., R. Woo., and S. Nandi. 1998. Ammonia abundance in Jupiter's atmosphere derived from the attenuation of the Galileo probe's radio signal. *J. Geophys. Res.* **103**, 22,847 - 22,855.

Gillett, F. C and W. J. Forrest. 1974. *Astrophys. J. Lett.* **187**, L39.

Grossman, A. W., D. O. Muhleman and G. L. Berge. 1989. High-resolution microwave images

of Saturn. *Science* **245**, 1211-1215.

De Graauw, T., H. Feuchtgruber, B. Bézard, P. Drossart, T. Encrenaz, D. A. Beintema, M. Griffin, A. Heras, M. Kessler, K. Leech, E. Lellouch, P. Morris, P. R. Roelfsema, M. Roos-Serote, A. Salama, B. Vandenbussche, E. A. Valentijn, G. R. Davis, and D. A. Naylor. 1997. First results of ISO-SWS observations of Saturn: Detection of CO_2, CH_3H_2H, C_4H_2 and tropospheric H_2O. *Astron. Astrophys.* **321**, L13 - L16.

Feuchtgruber, H., E. Lellouch, T. de Graauw, B. Bézard, T. Encrenaz, and M. Griffin. 1997. *Nature* **389**, 159 - 162.

Kaye, J. A.and D. F. Strobel. 1984. Phosphine photochemistry int eh atmosphere of Saturn. *Icarus* **59**, 314 - 335.

Levy, A., N. Lacombe, and G. Tarrago. 1993. Hydrogen-broadening and helium-broadening of phosphine lines. *J. Molec. Spectrosc.* **157**, 172 - 181.

Levy, A., N. Lacombe, and G. Tarrago. 1994. Temperature-dependence of collision-broadened lines of phosphine. *J. Molec. Spectrosc.* **166**, 20 - 31.

Lindal, G. F., D. N. Sweetnam, and V. R. Eshleman. 1985. The atmosphere of Saturn: An analysis of the Voyager radio occultation measurements. *Astron. J.* **90**, 1136-1146.

Loewenstein, R. F., D. A. Harper, S. H. Moseley, C. M. Telesco, H. A. Thornson, R. H. Hildebrand, S. E. Whitcomb, R. Winston, and R. F. Stiening. 1977. Far-infrared and submillimeter observations of the planets. *Icarus* **31**, 315- 324.

Noll, K. S. and H. P. Larson. 1990. The spectrum of Saturn from 1990 to 2230 cm^{-1}: Abundances of AsH_3, CH_3D, CO, GeH_4, NH_3 and PH_3. *Icarus* **89**, 168 - 189.

Orton, G. 1983. Thermal infrared constraints on ammonia ice particles as candidates for clouds in the atmosphere of Saturn. *Icarus* **53**, 293 - 300.

Orton, G. S., B. M. Fisher, S. T. Stewart, A. J. Friedson, J. L. Ortiz, M. Marinova, W. Hoffmann, J. Hora, M. Ressler, S. Hinkley, V. Krishnan, M. Masanovic, J. Tesic, A. Tziolas, and K. Parija. 1998. The Galileo Probe entry site: Characteristics of the Galileo Probe entry site from earth-based remote sensing observations. *J. Geophys. Res.* **103**, 22,791 - 22,814.

Pickett, H. M., R. L. Poynter, and E. A. Cohen. 1992. Submillimeter, millimeter, and microwave spectral line catalogue. JPL Publ. 80-23, Rev. 3, Jet Propulsion Laboratory, Pasadena, California.

Prinn, R. G., H. P. Larson, J. J. Caldwell, and D. Gautier. 1984. Composition and chemistry of Saturn's atmosphere. In *Saturn* (T. Gehrels and M. S. Matthews, Eds.), pp. 88-149. Univ. of Arizona Press. Tucson.

Roellig, T. L., M. W. Werner, and E. E. Becklin. 1988. Thermal emission from Saturn's rings at 380 μm. *Icarus* **73**, 574 - 583.

Strobel, D. F. 1978. Aeronomy of Saturn and Titan. In *The Saturn System* eds. D. Hunten and D. Morrison (Washington: NASA Conf. Publ. 2068), pp. 185 - 194.

Tokunaga, A. T., H. L. Dinerstein, D. F. Lester, and D. M. Rank. 1980. The phosphine abundance on Saturn derived from new 10-micrometer spectra. *Icarus* **42**, 79 - 85.

Tokunaga, A. T., H. L. Dinerstein, D. F. Lester, and D. M. Rank. 1981. Erratum: "The phosphine abundance on Saturn derived from new 10-micrometer spectra (*Icarus* **42**, 79 - 85, 1980)". *Icarus* **48**, 540.

Ulich, B. L, J. R. Dickel, and I. dePater. 1984. Planetary observations at a wavelength of 1.32 mm *Icarus* **60**, 590 - 598.

Weisstein, E. W. and E. Serabyn. 1994. Detection of the 267 GHz J=1-0 rotational transition of PH_3 in Saturn with a new Fourier transform spectrometer. *Icarus* **109**, 367 - 371.

Weisstein, E. W. and E. Serabyn. 1996. Submillimeter line search in Jupiter and Saturn. *Icarus 123* **23**, 23 - 36.

Werner, M. W., G. Neugebauer, J. R. Houck and M. G. Hauser. 1980. One-millimeter brightness temperatures of the planets. *Icarus* **35**, 289 - 296.

Winkelstein, P., J. Caldwell, S. J. Kim, M. Combes, G. E. Hunt, and V. Moore. A determination of the composition of Saturnian stratosphere using IUE. 1983. *Icarus* **54**, 309 - 318.

FIGURE CAPTIONS

Figure 1. Brightness temperature spectra of Saturn's disk with normalization of radiances as described in the text. The sinusoid in the data between 240 and 250 GHz is an artifact of the data acquisition. We don't want you to think about that, so we've cut off lower frequencies. Models with H_2 collision-induced opacity only are shown for reference with the alternating dotted-dashed line. Models with constant PH_3 mixing ratios in the troposphere below a rapid falloff above the 100-mbar level are shown by the solid and dashed lines indicated in the legend. The NH_3 mixing ratio is presumed to be a constant value of 1 x 10^{-4} below the saturation level in these models, but the dotted lines show the effect of changing this value between extremes of 3 x 10^{-5} (upper curve) and 4 x 10^{-4} (lower curve) for the nominal PH_3 model.

Figure 2. Vertical distribution of PH_3 for the models shown in Fig. 1. The line styles are the same as those in Fig. 1. The temperature structure assumed is shown for reference by the dotted line.

Figure 3. Vertical distribution of PH_3 as in Fig. 2, but for a constant log mixing ratio *vs* log pressure relationship. Note the cutoff given by the dashed line is inconsistent with the data (see Fig. 4), but the alternative (100-mbar) cutoff or the simple extension of the tropospheric mixing ratio *vs* pressure relationship into the stratosphere, both shown by solid curves, are consistent with the spectrum. The vertical line starting at the 630-mbar level shows the lower limit of the mixing ratio at depth that marginally matches our data at the 1-σ level. We adopt the extension of the tropospheric mixing ratio *vs* pressure relationship at all levels as our nominal model. The $\pm$25% uncertainty in the mixing ratio that arises from the noise and the slight inconsistency between the two data sets is illustrated by the two horizontal bars.

Figure 4. Spectra of the models shown in Fig. 3, compared with our data. The same linestyles are used to denote the models as in Fig. 3.

Figure 5. Weighting functions of the outgoing radiance associated with the model shown in Fig. 3 with the PH_3 cutoff pressure at 10 mbars. PH_3 1-0 transition weighting functions are offset to the right arbitrarily and displayed by thicker lines for clarity. The secondary peaks are the result

of the background continua arising from NH_3 line wing or H_2 collision-induced opacities.

Figure 6. Spectra of a perturbation of the model shown in Fig. 3 with temperature profile 2 Kelvins lower than the best fit linear model and the mixing ratio 25% lower than the same model, shown as the solid line. The Spectrum of the model shown in Fig. 3 is displayed for comparison as the dashed line.

Figure 7. Vertical distributions of PH_3. The standard model is given by the solid curve with thicker line indicating the vertical range to which our data are sensitive. The PH_3 distribution derived by Courtin *et al.* (1984) with a constant mixing ratio up to the 3-mbar level appears as a uniform mixing ratio in the pressure regime of this graph; it is given by the dashed-dotted line. The PH_3 distribution derived from the ISO SWS spectrum of Saturn (deGraauw *et al.* 1997) is shown by the dashed line.

Figure 8. Spectra of the models shown in Fig. 7 with our data. The same linetype for each model is used as in Fig. 7.

Figure 9. Vertical distributions of PH_3. The standard model is displayed as in Fig. 7. The vertical distribution of PH_3 derived by Noll and Larson (1990) is given by the dashed line. A modification that fits our data better is shown by the dashed-dotted line.

Figure 10. Spectra of the models shown in Fig. 9 with our data. The same linetype for each model is used as in Fig. 9. Where not apparent, the dashed-dotted line indicating our modification of the Noll and Larson profile is indistinguishable from our standard model.

Figure 11. Vertical profile of the PH_3 mixing ratio as a function of the eddy diffusion coefficient in the upper troposphere. The profile corresponding to 10^5 cm^2 sec^{-1} matches the standard model (Fig. 7) best between about 1 bar and 100 mbar.

Figure 12. Rate profiles corresponding to reactions as shown (reactions R1, R2 and R3 in the text) that are responsible for removing PH_3 from the upper troposphere. These rates correspond to the steady-state solution of K = 10^5 cm^2 sec^{-1}.

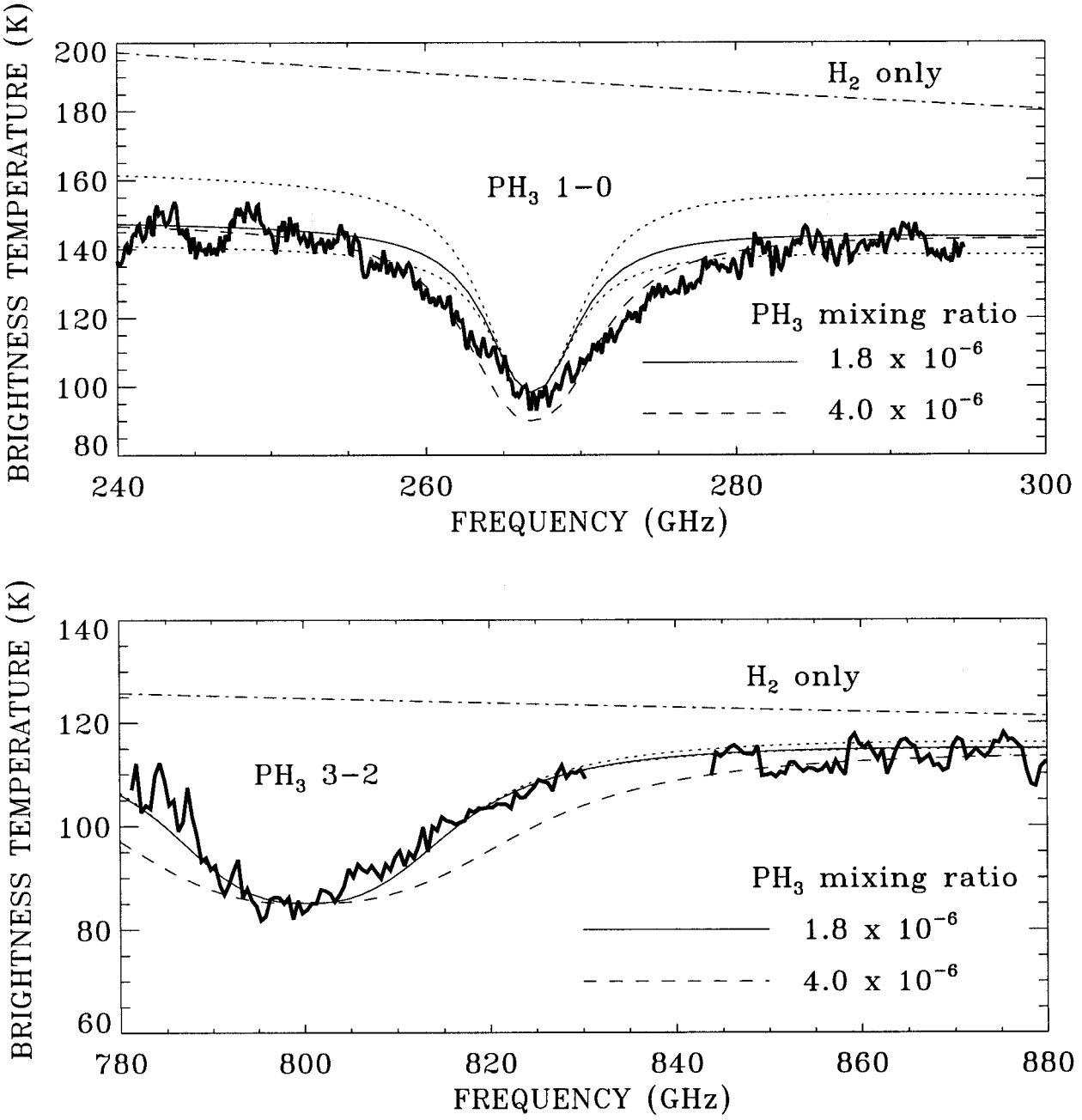
BRIGHTNESS TEMPERATURE (K)
200
180
160
140
120
100
80
240
260
280
300
FREQUENCY (GHz)
H2 only
PH3 1-0
PH3 mixing ratio
1.8 x 10-6
4.0 x 10-6
BRIGHTNESS TEMPERATURE (K)
140
120
100
80
60
780
800
820
840
860
880
FREQUENCY (GHz)
H2 only
PH3 3-2
PH3 mixing ratio
1.8 x 10-6
4.0 x 10-6

Figure 1

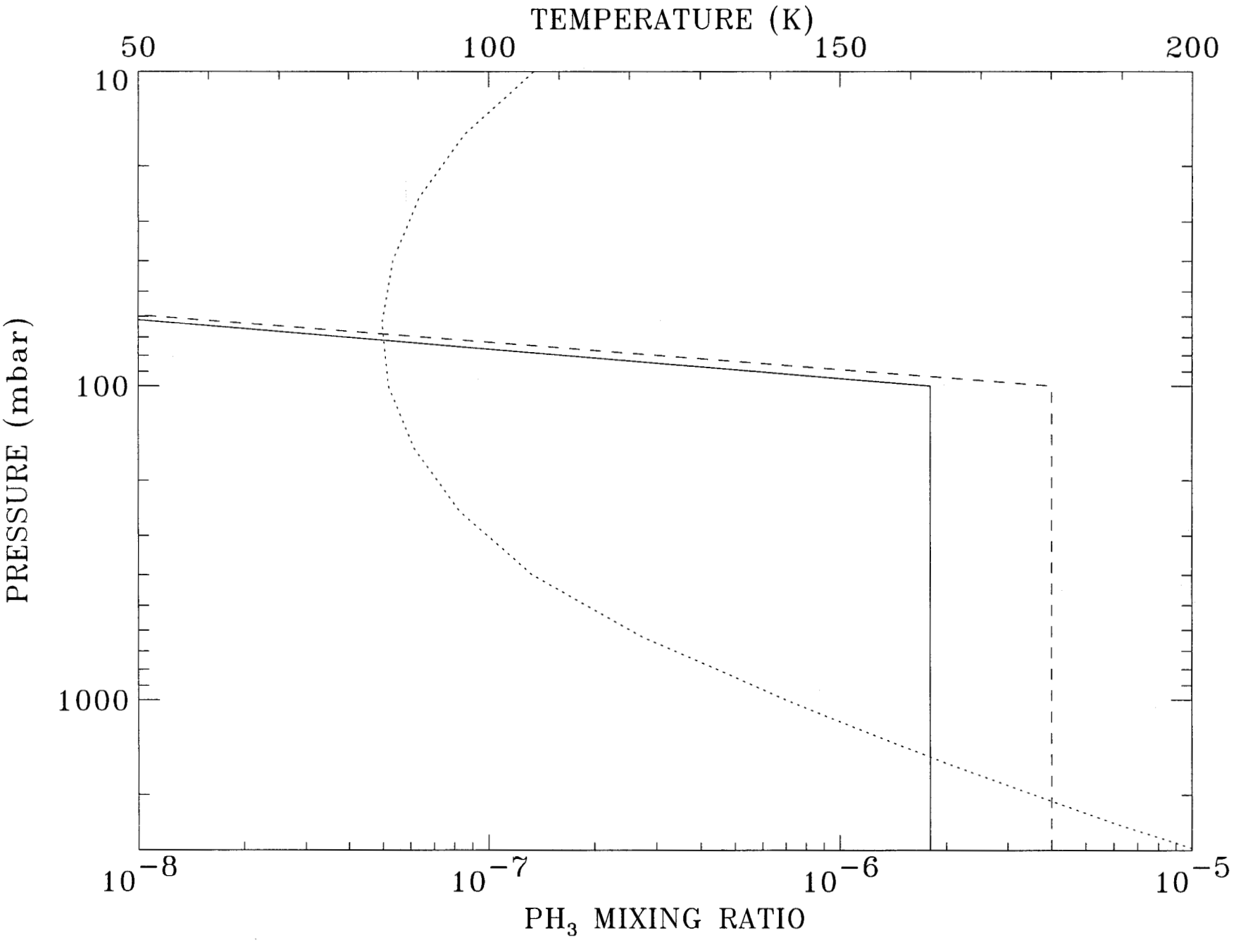
TEMPERATURE (K)
50
100
150
200
10
100
1000
PRESSURE (mbar)
10^{-8}
10^{-7}
10^{-6}
10^{-5}
PH_3 MIXING RATIO

Figure 2

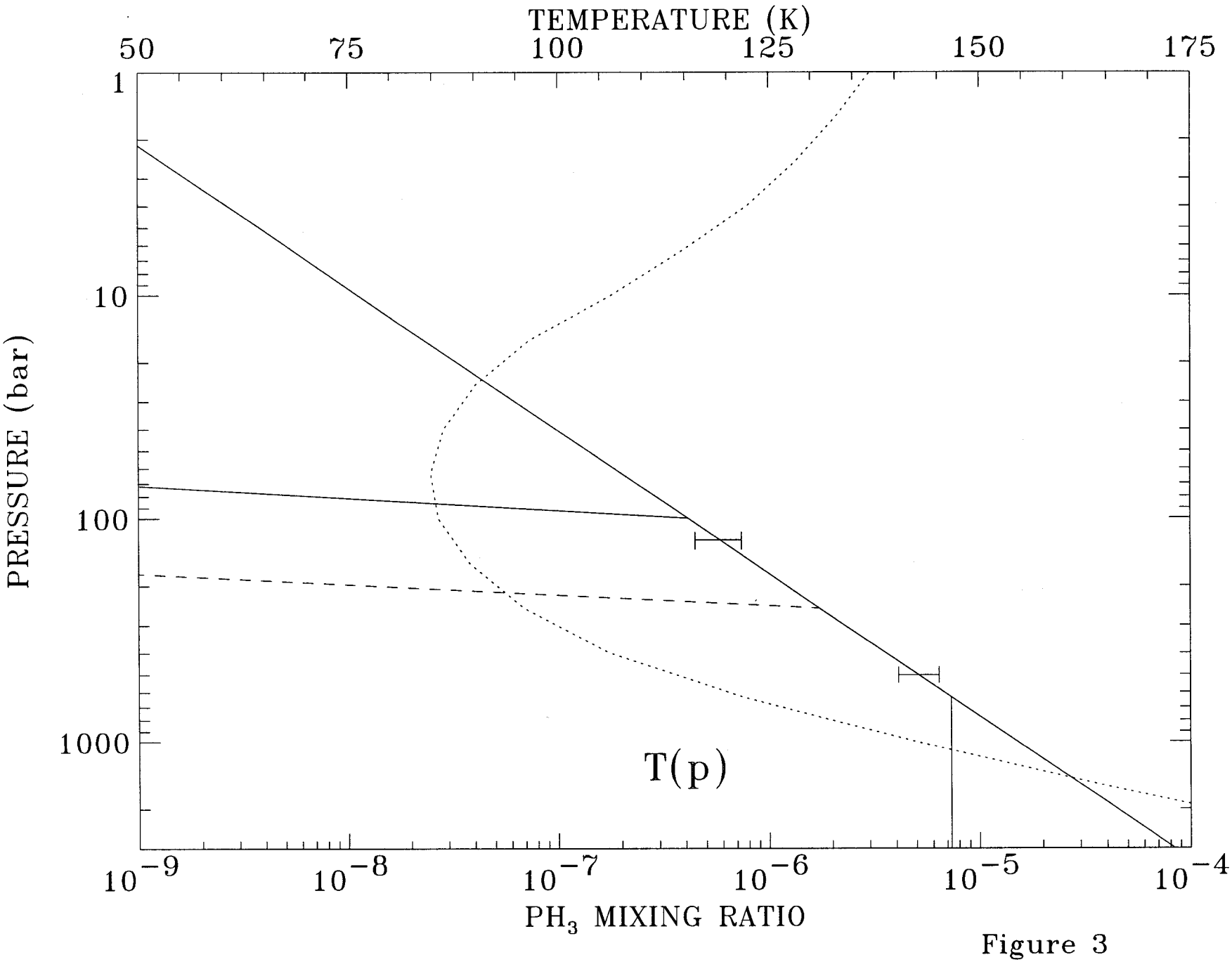
TEMPERATURE (K)
50
75
100
125
150
175
1
10
100
1000
PRESSURE (bar)
T(p)
10^{-9}
10^{-8}
10^{-7}
10^{-6}
10^{-5}
10^{-4}
PH_3 MIXING RATIO

Figure 3

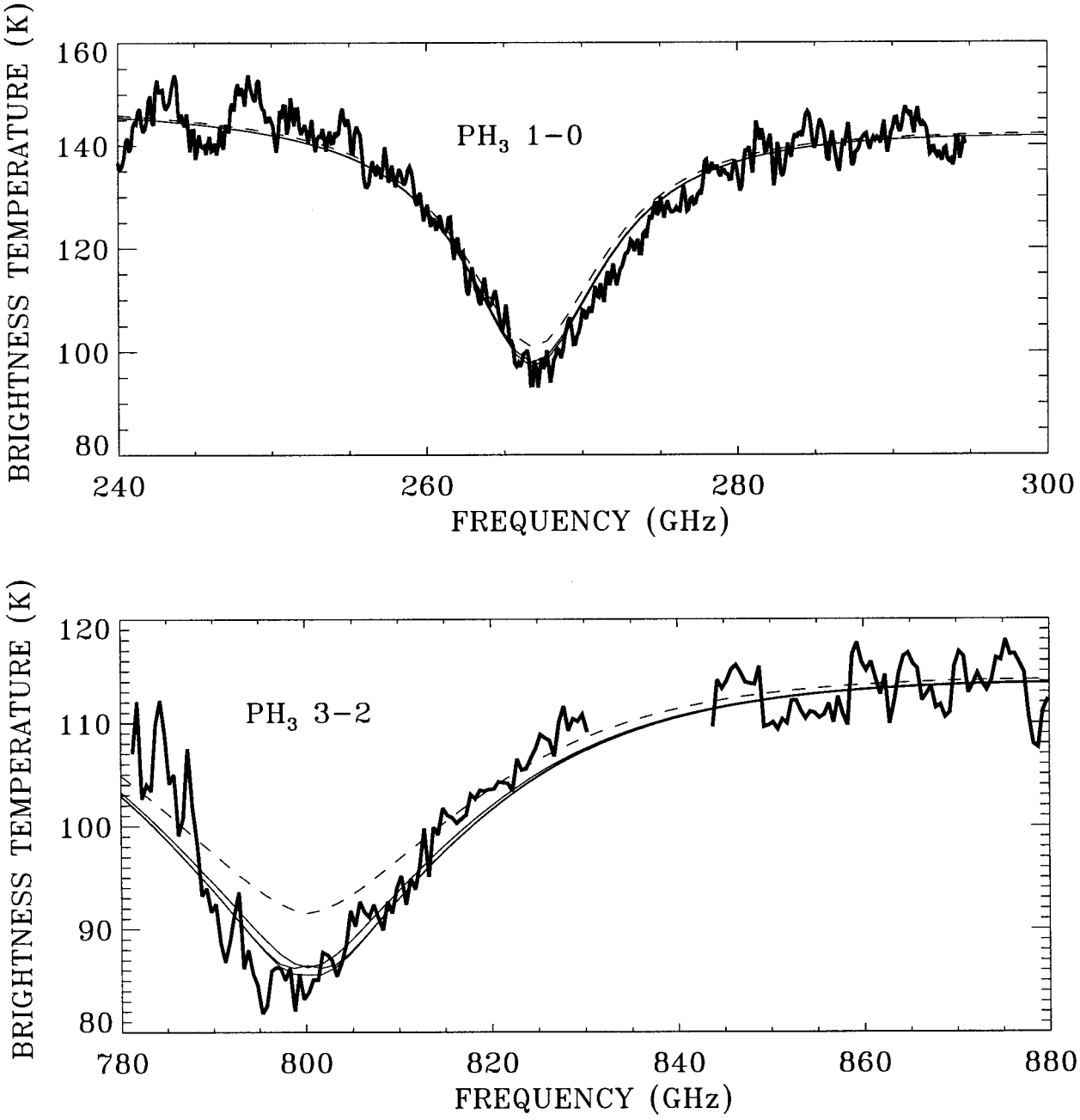
BRIGHTNESS TEMPERATURE (K)
160
140
120
100
80
PH3 1-0
240
260
280
300
FREQUENCY (GHz)
BRIGHTNESS TEMPERATURE (K)
120
110
100
90
80
PH3 3-2
780
800
820
840
860
880
FREQUENCY (GHz)

Figure 4

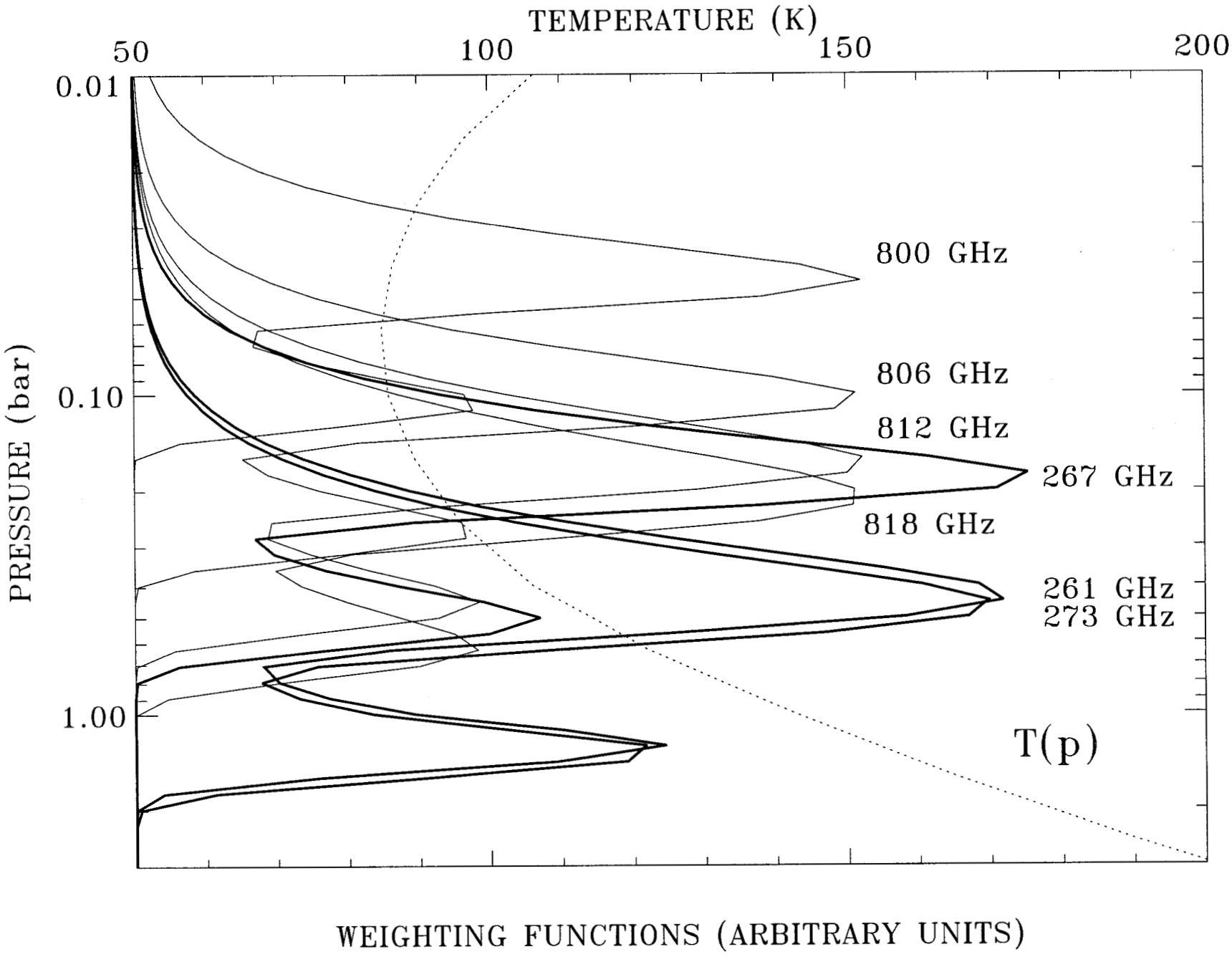
TEMPERATURE (K)
50
100
150
200
0.01
0.10
1.00
PRESSURE (bar)
800 GHz
806 GHz
812 GHz
267 GHz
818 GHz
261 GHz
273 GHz
T(p)
WEIGHTING FUNCTIONS (ARBITRARY UNITS)

Figure 5

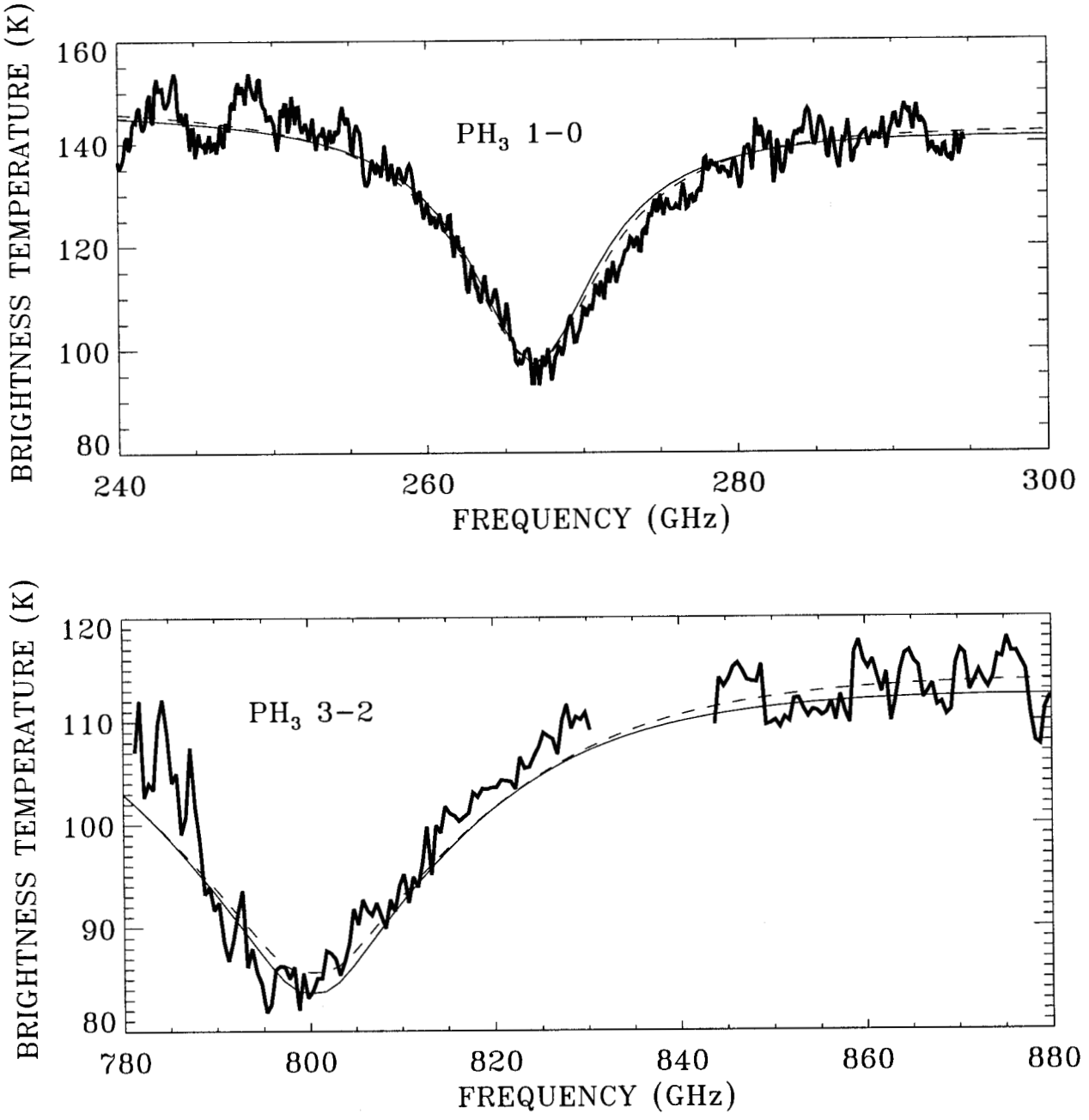
BRIGHTNESS TEMPERATURE (K)
160
140
120
100
80
PH3 1-0
240
260
280
300
FREQUENCY (GHz)
BRIGHTNESS TEMPERATURE (K)
120
110
100
90
80
PH3 3-2
780
800
820
840
860
880
FREQUENCY (GHz)

Figure 6

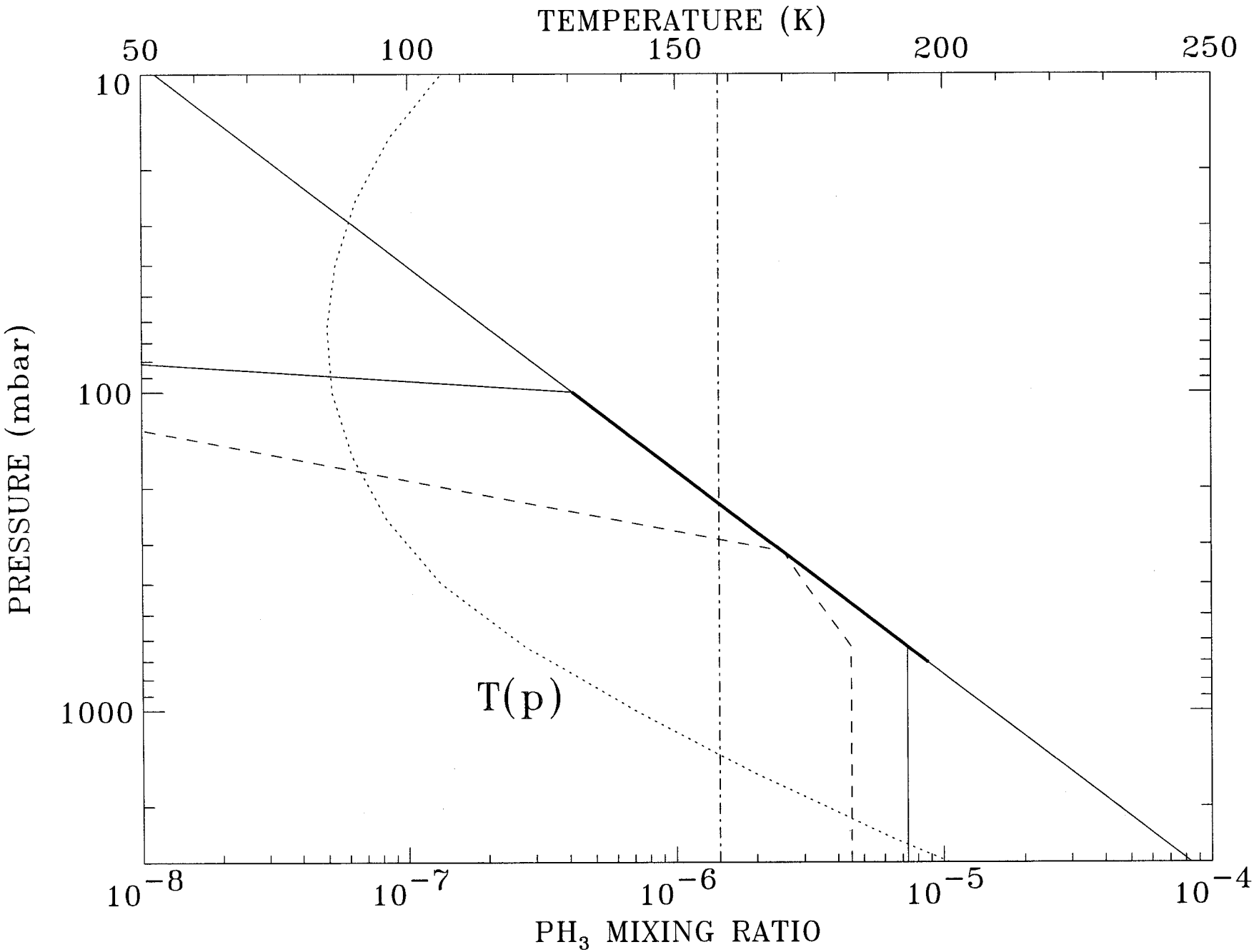
TEMPERATURE (K)
50
100
150
200
250
10
100
1000
PRESSURE (mbar)
T(p)
10^{-8}
10^{-7}
10^{-6}
10^{-5}
10^{-4}
PH_3 MIXING RATIO

Figure 7

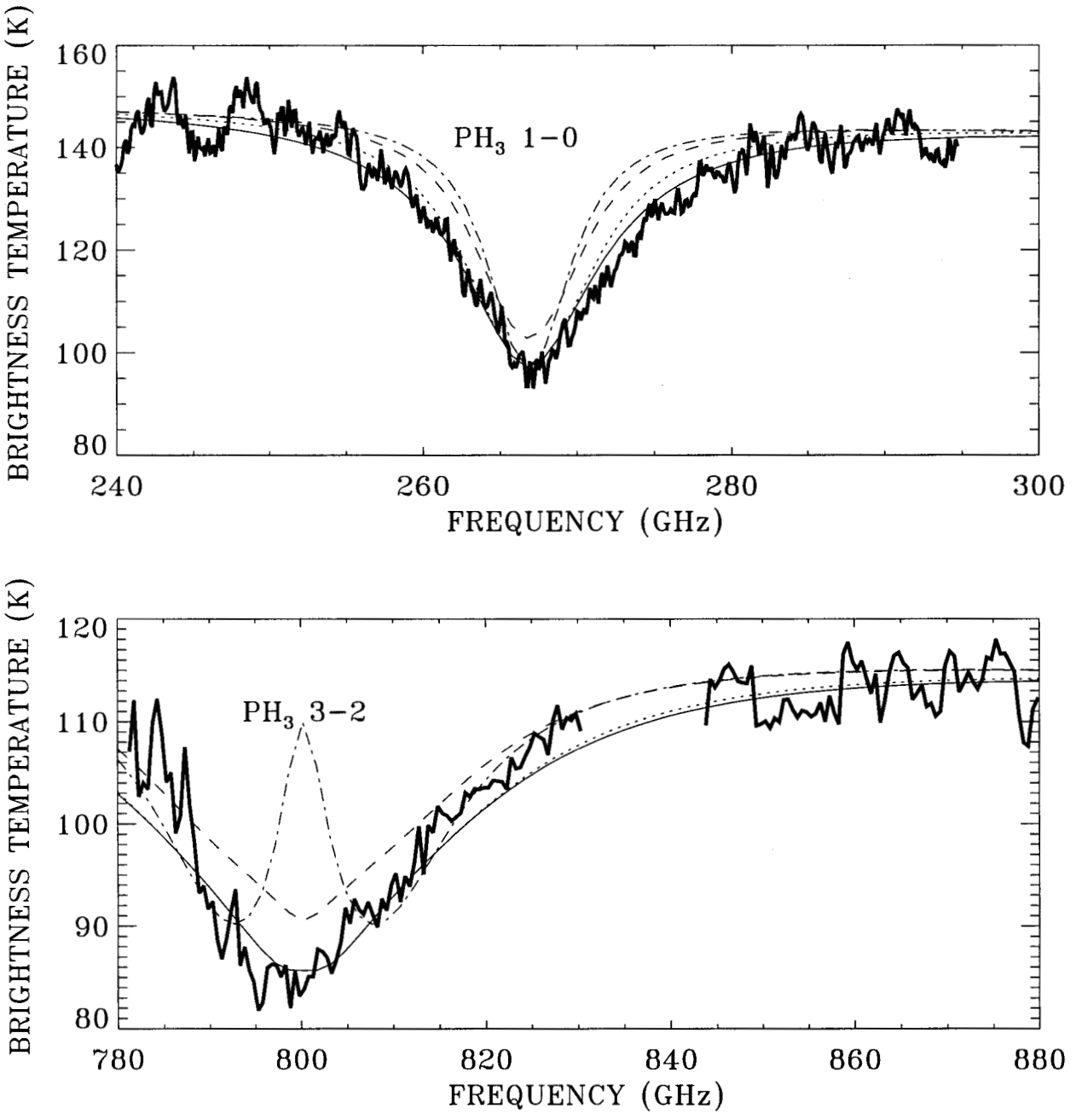
BRIGHTNESS TEMPERATURE (K)
160
140
120
100
80
PH3 1-0
240
260
280
300
FREQUENCY (GHz)
BRIGHTNESS TEMPERATURE (K)
120
110
100
90
80
PH3 3-2
780
800
820
840
860
880
FREQUENCY (GHz)

Figure 8

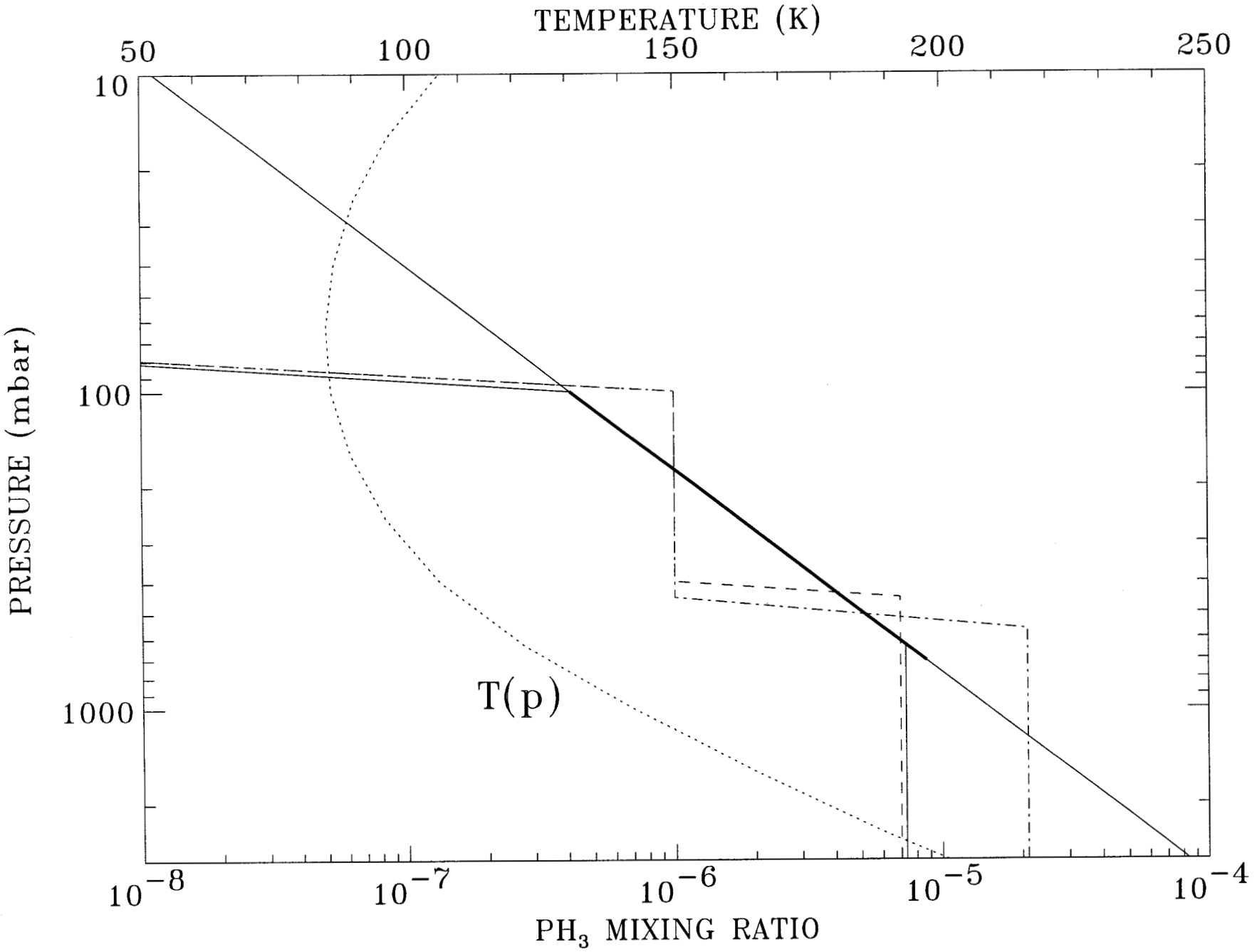
TEMPERATURE (K)
50
100
150
200
250
10
100
1000
PRESSURE (mbar)
T(p)
10^{-8}
10^{-7}
10^{-6}
10^{-5}
10^{-4}
PH_3 MIXING RATIO

Figure 9

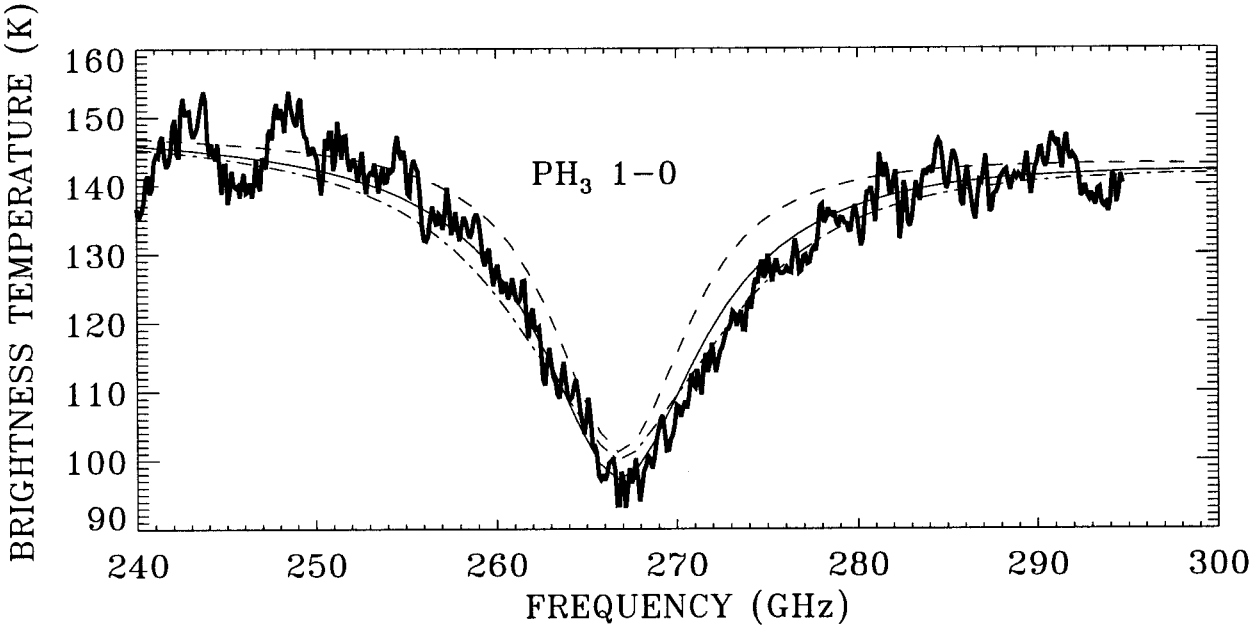
BRIGHTNESS TEMPERATURE (K)
160
150
140
130
120
110
100
90
PH3 1-0
240
250
260
270
280
290
300
FREQUENCY (GHz)

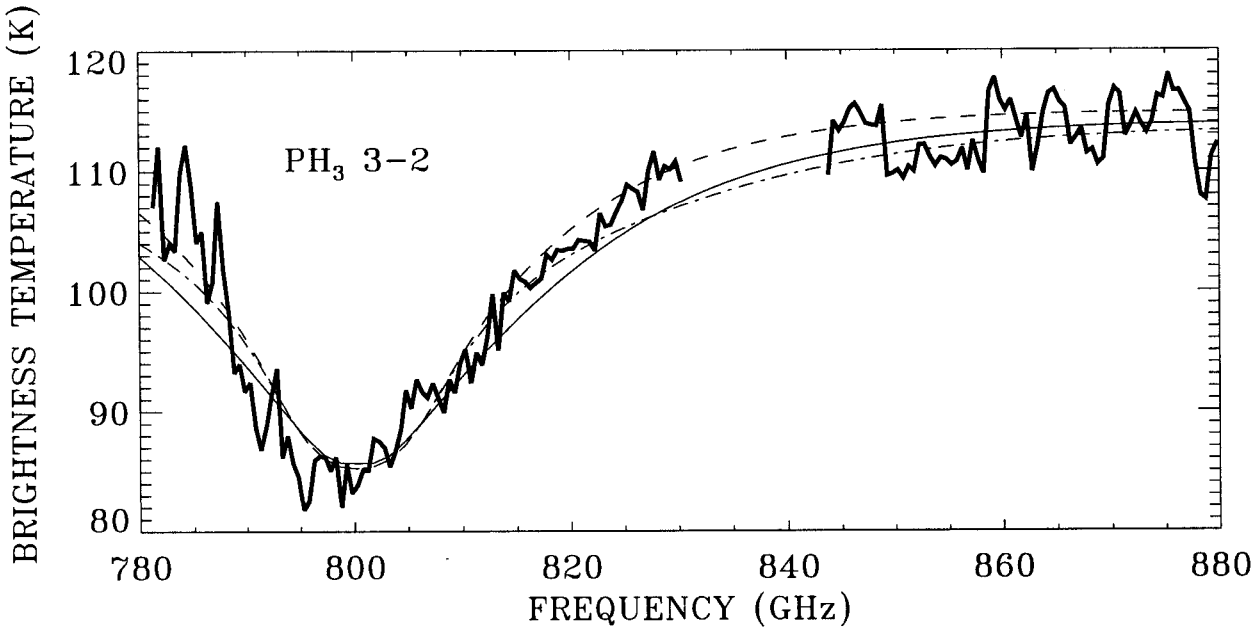
BRIGHTNESS TEMPERATURE (K)
120
110
100
90
80
PH3 3-2
780
800
820
840
860
880
FREQUENCY (GHz)

Figure 10

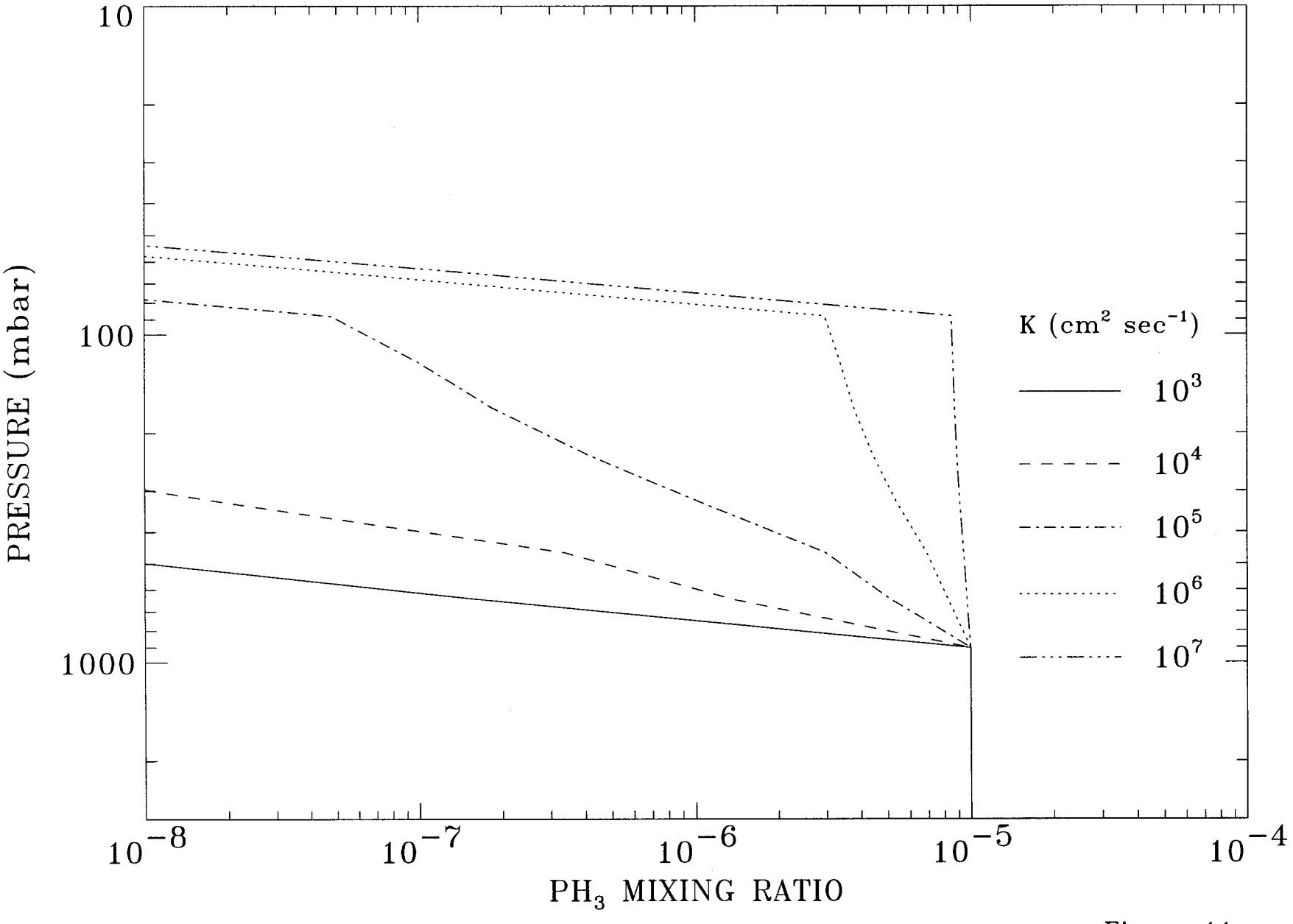
10
100
1000
PRESSURE (mbar)
10^{-8}
10^{-7}
10^{-6}
10^{-5}
10^{-4}
PH_3 MIXING RATIO
K (cm^2 sec^{-1})
10^3
10^4
10^5
10^6
10^7

Figure 11

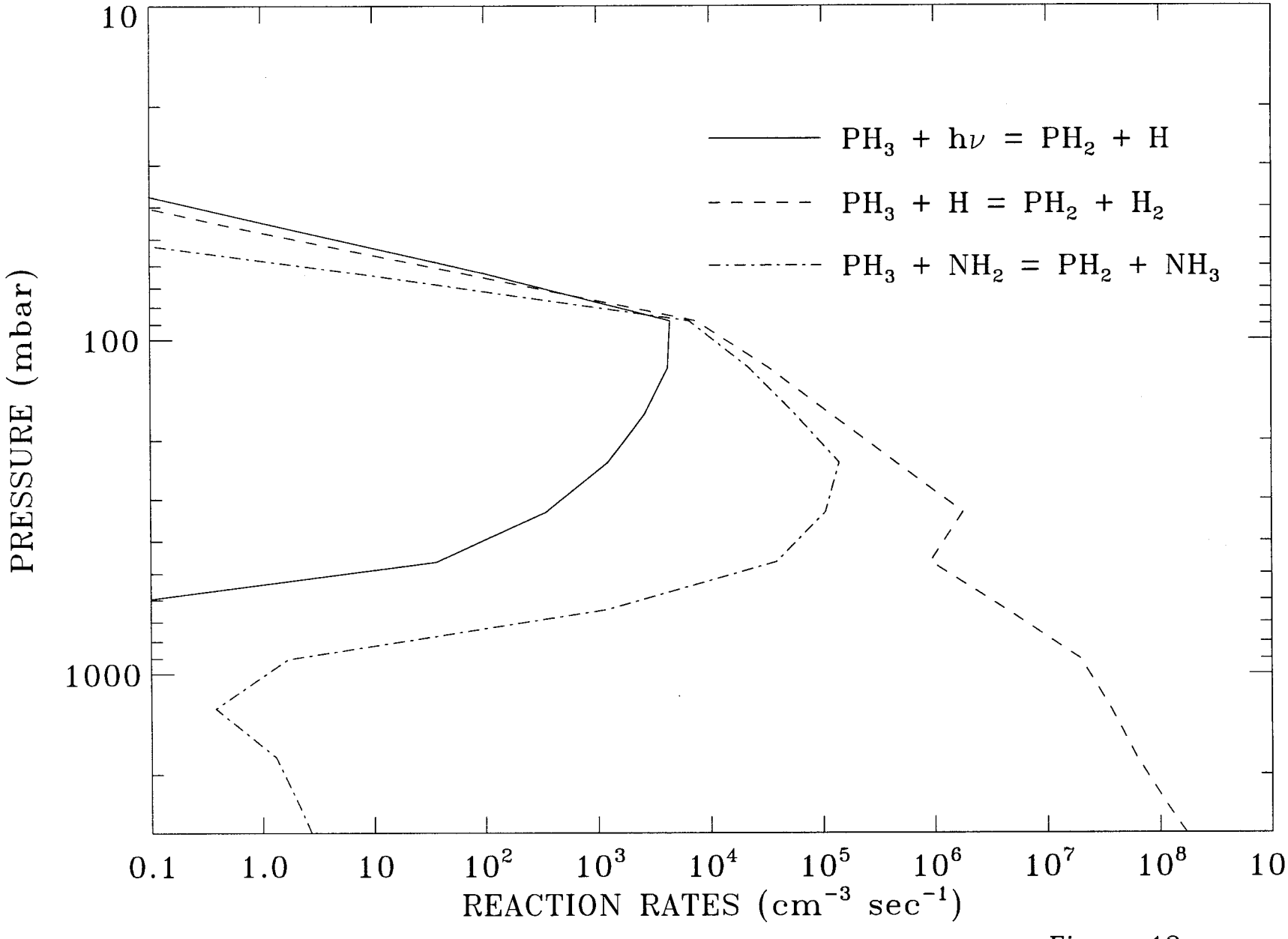
10
100
1000
PRESSURE (mbar)
PH3 + hν = PH2 + H
PH3 + H = PH2 + H2
PH3 + NH2 = PH2 + NH3
0.1
1.0
10
10^2
10^3
10^4
10^5
10^6
10^7
10^8
10^9
REACTION RATES (cm^-3 sec^-1)

Figure 12